

Sharp DNA denaturation in a 3D mesoscopic model

Mateus Rodrigues Leal^a, Gerald Weber^a

^a*Departamento de Física, Universidade Federal de Minas Gerais, 31270-901, Belo Horizonte-MG, Brazil*

Abstract

The mesoscopic Peyrard-Bishop DNA Hamiltonian describes the main molecular interactions with simple potentials, resulting in an efficient calculation of the melting of the duplex helix. It is based on a 2D model which can be simplified to calculate the classical partition function with the transfer-integral technique. At the heart of this approach are simplifications that leave only a single variable to integrate, but also make it impossible to apply the model to situations where a more detailed structural description is needed. Here, we start from a more realistic 3D description and work out several approximations to arrive at a form that can be handled by the transfer-integral technique. We show that this new approach naturally results very sharp opening transition.

Keywords: DNA stability, mesoscopic models, Peyrard Bishop model

1. Introduction

Simple models for describing nucleic acids always had an important role for understanding the underlying physics of these important type of biomolecules. For instance the Zimm-Bragg model [1] is one of the earliest theoretical approaches to describe the phase transitions in polypeptide chains providing much of the framework that was later applied to nucleic acids [2] and is in active use [3]. Statistical physics models using interaction potentials, instead of statistical weights, made a debut with Peyrard and Bishop [4] which added a completely new way to describe DNA with mesoscopic models. Its simplicity provides a computational efficiency that outcompetes atomistic simulations for describing melting in DNA [5]. Evidently, the increased efficiency comes at the expense of lack details describing the intramolecular interactions, but we

*Corresponding author

Email address: gweberbh@gmail.com (Gerald Weber)

showed that with a suitable approach combining the mesoscopic model with experimental data it is possible to overcome several of those limitations [6, 7]. In recent years, our group used the mesoscopic Peyrard-Bishop (PB) model to handle numerous nucleic acids systems, for instance to describe deoxyinosine [8], GU mismatches in RNA [9] and DNA-RNA hybrids [10]. Many of our findings correlate well with existing structural data from NMR and X-ray measurements providing a good level of validation for this theoretical approach.

The successful description of the melting process of various types of nucleic acids is a major motivation for improving the model without giving up its computational efficiency that makes it so useful. Perhaps the most important limitation of the original PB model is that it was set up as a purely two dimensional (2D) model [4]. The PB model represents the DNA molecule as being outright flat, that is, without its characteristic helical structure. It takes into account the transversal hydrogen bond and the longitudinal stacking interaction. The model introduces several simplifications that leaves only a single degree of freedom, transversal to the helical axis, and for this reason it also referred to as a 1D model [11, 12]. To avoid confusion, we will use the 2D and 3D terminology only in regard to the spatial dimensions of the interactions considered by the model, and not to describe the remaining degrees of freedom after simplifications or restrictions.

One of the possible reasons that explains why the PB model works so well is that near the melting transition temperature the molecule largely unwinds, as otherwise the strand dissociation would not be possible at all. Therefore assuming a flat molecule may not be such preposterous simplification. Evidently, there were several attempts to remove this constraints which led to the proposal of three dimensional (3D) model Hamiltonian, and within the framework of the mesoscopic description with interaction potentials [13, 14]. These models introduce the helical twist angle but require additional constraints to reduce the degrees of freedom, however they do not calculate the average strand opening with the transfer integral which is the aim of this work. It is noteworthy to mention that if one starts from one of these 3D Hamiltonians and simply set the angles to zero, as is if one flattens the 3D model to a 2D space, one does not regain the form of the original PB Hamiltonian [15].

Our aim is to adapt the 3D Hamiltonian and bring it within the reach of the transfer integral (TI) technique for calculating the average strand opening. The TI technique was developed for

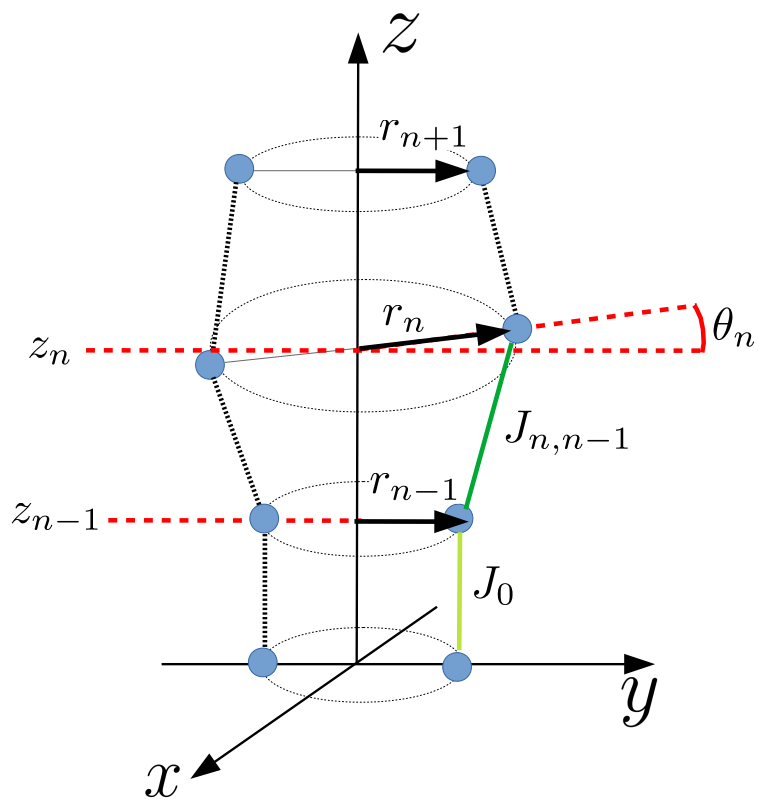


Figure 1: Schematic diagram of the 3D model. Dotted black lines show the stacking interaction between neighbouring bases, in particular the distance $J_{n,n-1}$ between the n -th and $n - 1$ -th bases is shown as a green line. The equilibrium distance J_0 is shown as a dark yellow line parallel to the z -axis.

systems with nearest-neighbour interactions [16] and is especially well suited for handling the intramolecular interactions in DNA-type systems as it dramatically reduces the numerical effort for calculating the classical partition function. The main challenge here is to find suitable approximations to the multiple integrals of the classical partition function in such a way that the only one dimension remains that can be handled by the TI technique. For the original 2D model this was achieved replacing variables describing the strand displacements by two relative in-phase and out-of-phase displacements [4]. In this case the in-phase displacement could be readily integrated, and the remaining out-of-phase variable was handled via the TI. For the 3D Hamiltonians the common approach is to fix the distance along the axis of the helix between neighbouring base-pairs, $z_{n+1} - z_n = h$ shown in fig. 1, known as the helical rise distance [17]. By fixing the rise distance, only the radial distance r and the twist angle θ need to be integrated. The angle integration was performed in several different ways, leaving the radial distance integration to be performed by TI [13, 18, 19]. However, fixing the rise distance effectively disallows any motion along the helical axis, the z -axis in Fig. 1, and therefore is still a major limitation. Other helicoidal models based on the PB Hamiltonian that do not calculate melting transitions or employ different calculation methods, such as refs. [20–25], are not covered here.

Here, we are considering the 3D PB Hamiltonian [13, 18] but without prior fixing the rise distance. As we will see, relaxing this conditions requires the introduction of other constraints, in particular we will restrict the z -motion, fig. 1, to small amplitudes. In addition, we will consider small twist angles considering that near the melting transition the duplex should unwind almost completely. The small twist angle also resembles the ‘nearly-flat’ scenario used for the 2D model and therefore provides an interesting basis for comparison between the nearly-flat-3D and 2D model. Apart from these constraints we had to introduce a number of additional approximations that would allow us to integrate over z and θ and arrive at a form that could be finally be handled by the TI technique. To fully evaluate the influence of those approximations we also numerically integrated the complete configurational part of the partition function. These numerical tests show that the results from the approximated 3D Hamiltonian are qualitatively similar to the unapproximated ones, and therefore a step forward compared to 2D models, for the study of melting transitions in DNA.

2. Model

The configurational part of the classical partition of a oligonucleotide duplex composed of N base-pairs is written in terms of the polar cylindrical coordinates z , r and θ

$$Z_{r\theta z} = \Gamma^N \int \prod_{n=1}^N dz_n d\theta_n r_n dr_n e^{-\beta U_{n,n-1}(z_n, \theta_n, r_n)} \quad (1)$$

where $\beta = 1/(k_B T)$, k_B is the Boltzman constant and T the absolute temperature. Γ is a density factor, which is taken here as a reciprocal unit of volume, such that $Z_{r\theta z}$ becomes adimensional. U is the configurational part of model Hamiltonian and is a function of z , θ and r . The customary periodic boundary condition, where the last base-pair interacts with the first, is represented by the potential $U_{1,N}$. The average radius $\langle r_k \rangle$, representing the intra-strand opening, can be calculated as follows

$$\langle r_k \rangle = \frac{\Gamma^N}{Z_{r\theta z}} \int \prod_{n=1}^N r_k dz_n d\theta_n r_n dr_n e^{-\beta U_{n,n-1}} \quad (2)$$

For the case where all model parameters are the same at each site k , we have $\langle r \rangle = \langle r_1 \rangle = \dots = \langle r_N \rangle$.

For all r_n and θ_n the integrations are taken within the limits $r_n \in [0, b]$, $\theta_n \in [-\Theta, \Theta]$. For z we integrate within a region $\pm\zeta$ around the rise distance h_0 such that the limit is taken as

$$z_n \in [(n-1)h_0 - \zeta, (n-1)h_0 + \zeta] \quad (3)$$

the partition function is then written with explicit integration limits as

$$Z_{r\theta z} = \Gamma^N \int_0^b \int_{-\Theta}^{\Theta} \int_{(n-1)h_0 - \zeta}^{(n-1)h_0 + \zeta} \prod_{n=1}^N dz_n d\theta_n r_n dr_n \exp[-\beta U_{n,n-1}(z_n, \theta_n, r_n, z_{n-1}, \theta_{n-1}, r_{n-1})] \quad (4)$$

where each integration symbol implies N -uple integrals.

The interaction potential U is divided into stacking interactions $W_{n,n-1}$ and base-pair interactions V_n ,

$$U_{n,n-1}(z_n, \theta_n, r_n, z_{n-1}, \theta_{n-1}, r_{n-1}) = V_n(r_n) + W_{n,n-1}(z_n, \theta_n, r_n, z_{n-1}, \theta_{n-1}, r_{n-1}) \quad (5)$$

In terms of the polar cylindrical coordinates and considering the 3D scheme shown in fig. 1, the base-pair interaction potential is solely a function of r_n , that is $V_n(r_n)$ and it brings no difficulty for the integration of eq. (1),

$$V_n(r_n) = D \left\{ e^{-a(r-R_0)} - 1 \right\}^2 \quad (6)$$

where D is the depth of the potential, a the width and R_0 an equilibrium distance. The stacking interaction W however depends on all coordinates and links to consecutive base-pairs n and $n + 1$, which is the main point of difficulty for a full algebraic integration of the partition function, eq. (1). Therefore, our efforts will centre on the handling of the 3D stacking potential and, unlike the base-pair potential, the specific form of this potential is a crucial aspect of the theoretical method.

The stacking interaction potential is given by the harmonic potential between neighbouring bases n and $n + 1$,

$$W_{n,n-1} = \frac{k}{2} (J_{n,n-1} - J_0)^2, \quad (7)$$

where $J_{n,n-1}$, shown as a green line in fig. 1, is the distance between two bases, J_0 is the equilibrium distance, and k the elastic constant. In polar cylindrical coordinates z , r and θ , shown in fig. 1, the distance $J_{n,n-1}$ is written as

$$J_{n,n-1} = \sqrt{\Delta z_{n,n-1}^2 + f_{n,n-1}^2} \quad (8)$$

where $f_{n,n-1}$ is the xy -projection

$$f_{n,n-1} = \sqrt{r_n^2 + r_{n-1}^2 - 2r_n r_{n-1} \cos(\omega + \theta_n - \theta_{n-1})} \quad (9)$$

The equilibrium distance between the two consecutive base-pairs along the z -axis is h_0 , corresponding to the rise distance and ω is the structural twist angle [17]. For simplicity, we will assume that both bases at the n th site are at the same distance in regard to the z axis, that is, they move symmetrically with respect to the helical z axis. While this may seem overly restrictive, we have shown that for the classical partition function in the 2D system this means that the elastic constant is simply the average of the elastic parameters of each strand [26]. Therefore, the elastic constant k is the equivalent constant of the two springs to each side of the duplex strand. In terms of the DNA structure, the base pairs of a B-DNA helix have almost no slide and no inclination,

that is they are centred and perpendicular to the helical axis [17]. Therefore, our description is reasonable for B-DNA, but probably not for A-DNA.

We now expand eq. (8) to first order of $\Delta z_{n,n-1}^2$

$$J_{n,n-1} \approx \Delta z_{n,n-1} \left[1 + \frac{1}{2} \frac{f_{n,n-1}^2}{\Delta z_{n,n-1}^2} \right]. \quad (10)$$

Naturally, one can perform the algebraic development to higher orders of $\Delta z_{n,n-1}^2$, but it renders the remaining equations much more complicated. Therefore, for the sake of the discussion, we will present here only the simpler development following the first order expansion without loss of generality, and show the more complicated expansion to second order in supplementary equations Eqs. (S1–S3).

The equivalent equations to the second order expansion are shown in the supplementary material. We now use the additional restriction

$$\Delta z_{n,n-1} \approx J_0 \quad (11)$$

which is necessary for the integration in z , and the partition function simplifies to

$$Z_{r\theta z} = \Gamma(2\zeta)^N \int_0^b \int_{-\Theta}^{\Theta} \prod_{n=1}^N dr_n d\theta_n r_n e^{-\beta V(r_n)} \exp\left(-\beta k \frac{f_{n,n-1}^4}{4J_0^2}\right) \quad (12)$$

For the angle integration we will use the approximation

$$\cos(\omega + \theta_n - \theta_{n-1}) \approx 1 - \frac{\omega^2}{2} \quad (13)$$

and integrating over θ , we arrive at the final approximated form of the partition, after rearranging terms to symmetrize the integrand function

$$\begin{aligned} Z_{r\theta z}^{app.} &= \Gamma^N(4\zeta\Theta)^N \int_0^b \prod_{n=1}^N dr_n \sqrt{r_n r_{n-1}} \exp\left\{-\frac{\beta}{2} [V(r_n) + V(r_{n-1})]\right\} \\ &\quad \times \exp\left[-\beta k \frac{(r_n - r_{n-1})^4}{4J_0^2}\right] \exp\left[-\beta k \frac{r_n^2 r_{n-1}^2 \omega^4}{4J_0^2}\right] \end{aligned} \quad (14)$$

Note that the fluctuations along and around the z -axis are given by ζ and Θ , respectively, which are now outside the remaining integration, therefore those factors will simply cancel out when calculating expectation values, eq. (2).

The remaining variable to integrate is in r_n which can be handled by the transfer integral technique where the kernel is

$$K(x, y) = (xy)^{1/2} e^{-\frac{\beta}{2}[V(x)+V(y)]} \exp\left[-\beta k \frac{(x-y)^4}{4J_0^2}\right] \exp\left[-\beta k \frac{x^2 y^2 \omega^4}{4J_0^2}\right] \quad (15)$$

2.1. Numerical tests

To verify the impact of the successive approximations we will perform a numerical integration of the complete partition function, eq. (4), and compare it to the final approximated partition function, eq. (14). The numerical evaluation of eq. (4) will be carried out for the smallest possible number of base pairs, $N = 2$, which requires the numerical evaluation of a 6-tuple integral and as well as substantial computational resources. Nevertheless, considering a homogeneous DNA sequence, $N = 2$ is sufficient for our purposes. We will keep the periodic boundary condition, may seem odd for a sequence of length of just $N = 2$, however there is no loss of generality for the results presented here. The reason for this is that a sequence of length $N = 2$ has two elastic constants, $k_{1,2} = k_{2,1} = k$, where the last one represents the periodic boundary condition. The open boundary condition is simply setting $k_{1,2} = k$ and $k_{2,1} = 0$ [27], which for $N = 2$ turns out to be the exact equivalent of maintaining the periodic boundary condition and setting $k_{1,2} = k_{2,1} = k/2$.

We will designate the partition function calculated from eq. (4) in this way as Z_C , where C stands for complete,

$$Z_C = Z_{r\theta\zeta}[N = 2, b, \zeta, \Theta] \quad (16)$$

Furthermore, we calculate eq. (16) by adding the restrictions of eqs. (11) and (13), we will call this the restricted (R) calculation, which is a subset of the Z_C calculation,

$$Z_R = Z_C \left[\Delta z_{n,n-1} \approx J_0; \cos(\omega + \theta_n - \theta_{n-1}) \approx 1 - \frac{\omega^2}{2} \right] \quad (17)$$

For all numerical calculations we use the Gauss-Legendre quadrature. The integration steps were 1500 for a fixed b , which is the most critical integration due to the occurrence of numerical instabilities and divergences. For the varying integration limit b we used the rule of $200 + 60(b/\text{nm})$ integration points. For ζ and Θ , 10 integration points were found to be sufficient for achieving numerical convergence.

The approximated partition function eq. (14) can be evaluated via the transfer integral (TI) technique [4, 27]. In this technique the kernel is discretized over M points in the interval $[0, b]$, resulting in a $M \times M$ symmetrical matrix which is diagonalised, resulting in M eigenvalues λ_i , such that the resulting partition function becomes

$$Z_{TI} = \Gamma^2(4\zeta\Theta)^2 \sum_i^M \lambda_i^2 \quad (18)$$

The average radius $\langle r \rangle_{TI}$ is calculated as

$$\langle r \rangle_{TI} = \frac{\sum_i^M \lambda_i^2 \int_0^b |\phi_i|^2 dr}{\sum_i^M \lambda_i^2} \quad (19)$$

where ϕ_i are the eigenfunction. For details of this procedure see Refs. [4, 27, 28]. We will refer to the approximation calculated by the TI technique as T1 and T2, for the first and second order expansion of eq. (8).

Unless noted otherwise, for the numerical tests we used the following parameters: $D = 0.2$ eV, $a = 42.5$ nm⁻¹, $k = 4$ eV/nm², $J_0 = 0.7$ nm, corresponding to a homogeneous oligonucleotide sequence, and were largely chosen to highlight the main differences in the integration methods. The equilibrium distance was taken as $R_0 = 0.1$ nm, as r represents half the distance between the base pairs, this corresponds to a hydrogen equilibrium bond distance of $2R_0 = 0.2$ nm.

3. Results and discussion

The dependence of the average radius $\langle r \rangle$ as function of temperature is shown in fig. 2a for the three types of numerical tests, C, R, T1 and T2. In all cases, the denaturation curves exhibit the characteristic sigmoidal shape of the melting transition that has been the landmark of the Peyrard-Bishop model [4]. The approximated calculation to first order expansion, T1, underestimates the average radius when compared to the C and R calculations, especially as temperature increases. The restrictions represented by eqs. (11) and (13) do represent a substantial part of this reduction, as shown by the R calculation. This is to be expected as all three approximations, eq. (10,11,13), essentially limit the scope of the integration thus resulting in smaller $\langle r \rangle$. However, when we use the second order expansion T2, the result is very close to the R calculation, therefore the

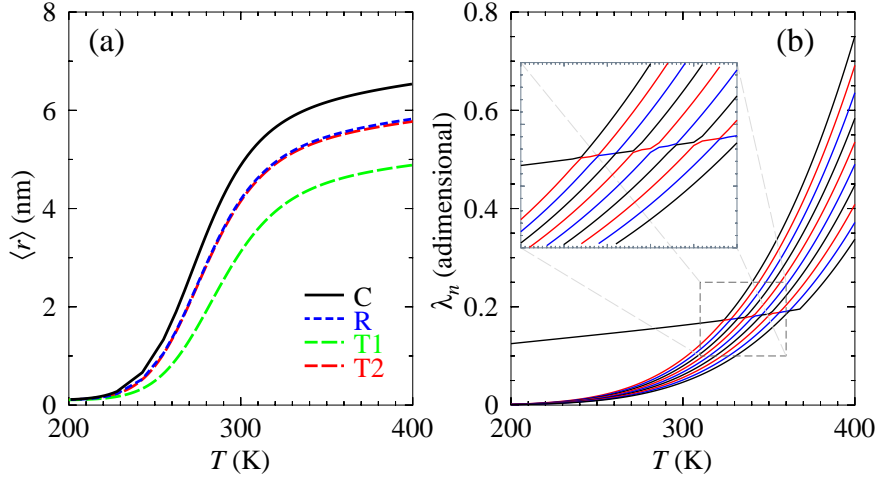


Figure 2: Panel (a): calculated average radius $\langle r \rangle$ as function of temperature for calculations of type C (black curve), R (blue short dashed), T1 (green long dashed) and T2 (red short dashed). Panel (b): 10 highest eigenvalues λ_n for T1 (T2 in fig. S1), the inset shows a zoom-in to highlight the anti-crossings. Integration limits are $\zeta = 10^{-2}$ nm, $\omega = 0.05$ rad, $\Theta = 0.01$ rad and $b = 20$ nm.

differences between T1 and R are only due to the order of the expansion of eq. (8). The spectrum of λ_n for T1 is shown in fig. 2b (see fig. S1 for T2) and displays the characteristic anti-crossing between successive eigenvalues [12], which is highlighted in the zoomed-in inset. Unlike the spectra of the 2D models [29] where the eigenvalues have a substantial gap at the anti-crossings, here in fig. 2b this gap is hardly noticeable.

Note that the transition shown in fig. 2 is very broad for all cases, this due to the fact that the DNA sequence has only two base pairs, that is $N = 2$, a limitation imposed by the numerical evaluations of the R and C calculations. Sharp transitions were observed for the Dauxois-Peyrard-Bishop (DPB) Hamiltonian with an anharmonic term and by setting $N \rightarrow \infty$ [30]. In fig. 3a we show the dependence of $\langle r \rangle$ for a sequence of length $N = 25$ for T1 displaying an extremely abrupt transition, see fig. S2 for T2. Varying the Morse potential D changes the temperature where the transitions occurs but not the $\langle r \rangle$ at high temperatures. The stacking parameter k on the other hand has an influence on both the onset of the transition and the high temperature value of $\langle r \rangle$. For comparison, we shown in fig. 3b some examples of average displacements $\langle y \rangle$, the equivalent 2D quantity to the 3D $\langle r \rangle$. Clearly, the 3D model has a much steeper increase of $\langle r \rangle$.

To understand the differences between the 3D and 2D model it is instructive to look at the symmetrized kernel eq. (15) used for the T1 calculation, see supplementary eq. (S4) for T2, and compare with the 2D kernel [4, 5]

$$K_{2D}(x, y) = e^{-\frac{\beta}{2}[V(x)+V(y)]} \exp\left[-\beta k \frac{(x-y)^2}{2}\right] \quad (20)$$

One important difference is the $(x-y)^4$ in stacking term of eq. (15), instead of $(x-y)^2$ for the 2D kernel [4]. If one thinks of mapping the 3D kernel to a 2D configuration space, this would seem like introducing an anharmonic stacking. However, in our tests with the 2D model such a fourth power term is not the main cause a steep transition (data not shown), although it has an important influence on which temperature the transition starts and how large $\langle r \rangle$ becomes at higher temperatures. What actually ensures the abrupt rise of $\langle r \rangle$ is the $(xy)^{1/2}$ factor which comes from the added degree of freedom. It also has an effect on magnitude of the potential parameters. For instance, the D we used to obtain a transition at higher temperatures is much closer actual energies of the hydrogen bonds, between 0.15 and 0.4 eV [31, 32], whereas for the 2D model these potentials had to be an order of magnitude smaller. The last factor in eq. (15) contains the twist angle ω which plays a role in preventing the divergence in the integration, we will discuss this in more detail next.

All PB-type models suffer from a numerical divergence, this is becomes especially apparent for the anharmonic DPB model and was discussed in detail by Zhang *et al.* [27]. One tentative approach to circumvent this divergence is to add a twist angle ω to eq. (20) [5],

$$(x-y)^2 \rightarrow (x^2 - 2xy \cos \omega + y^2) \quad (21)$$

which mimics a small out of plane angle. This procedure avoids the divergence for any 2D model [29], but also reduces the steepness of the transition, see dashed curves fig. 3b. In general, the solvent-barrier (SB) model [29], another PB-model Hamiltonian, has a much steeper increase of the displacement than the anharmonic Dauxois-Peyrard-Bishop (DBP) [30] or the original harmonic PB model [4]. The 3D model is not immune to the divergence problem if the twist angle is zero, $\omega = 0$, as shown in fig. 4. The radius $\langle r \rangle$ diverges much more strongly than the partition function $Z_{r\theta z}$ due to the additional variable r in the integration of eq. (2). Therefore the onset of the

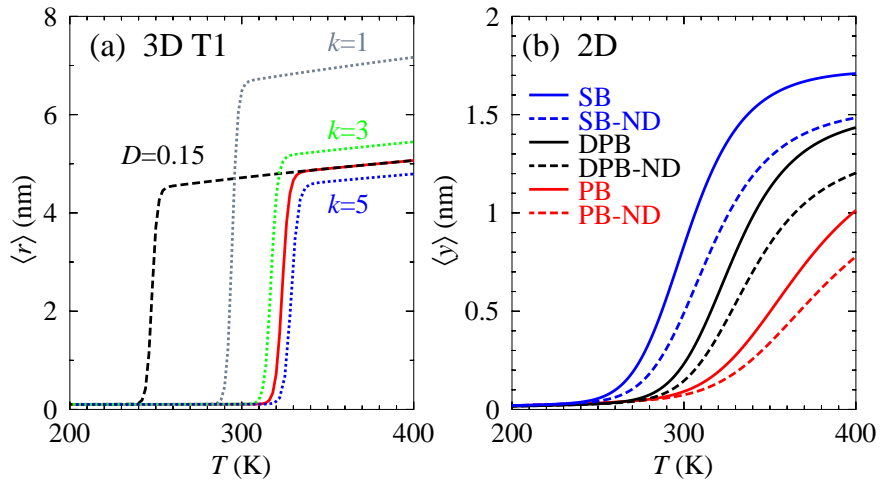


Figure 3: Calculated average radius $\langle r \rangle$ for T1 (panel a, for T2 see fig. S2) and calculated 2D average displacement $\langle y \rangle$ (panel b) as function of temperature for sequences of size $N = 25$. Panel (a): Morse parameters parameters are $D = 0.2$ eV for all curves, except dashed black curve for which $D = 0.15$ eV was used; Stacking parameters are $k = 4$ eV/nm² for the red solid curve and black dashed curve, the remaining dotted curves are indicated in eV/nm². Parameters for the T1 were $\zeta = 10^{-2}$ nm, $\omega = 0.05$ rad, $\Theta = 0.01$ rad and $b = 20$ nm. Panel (b): parameters for the 2D DPB model as in ref. [30], and for PB and SB as in ref. [29]. Also shown as dashed curves, with suffix ND (non-divergent), are the calculations with added angle $\omega = 0.01$ as in eq. (21).

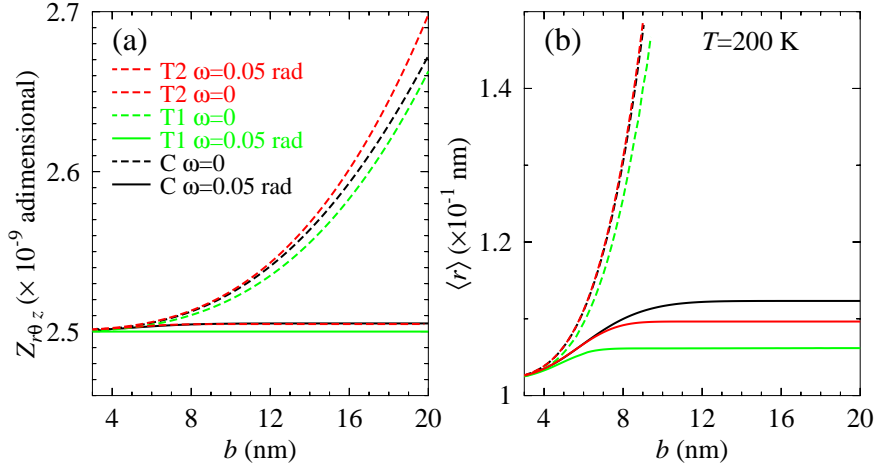


Figure 4: Calculated (a) configurational part of the partition function $Z_{r\theta z}$ and (b) average radius $\langle r \rangle$ as function of the upper limit b of the integration variable r , at 200 K, for C (black), T1 (green) and T2 (red). Full curves are for a twist angle of $\omega = 0.05$ rad and dashed curves for $\omega = 0$. Integration limits are $\zeta = 10^{-2}$ nm, $\Theta = 0.01$ rad.

divergence for $\langle r \rangle$, fig. 4b, occurs at a much shorter b than for $Z_{r\theta z}$, fig. 4a. The divergence appears equally for the C and T1 calculations, and consequently is not a particularity introduced by the approximations or by the transfer integral technique. Setting the twist angle ω to a non-zero value, no matter how small, removes the divergence entirely and therefore brings some justification to the similar approach used in the 2D model, eq. (21) [29].

The limit Θ of the angle θ and the upper limit ζ for the z variable both appear as constant factors in eq. (14) and therefore are cancelled in the calculation of the average radius. As a consequence, the average radius is constant for θ and ζ , for the approximated calculation as shown in fig. 5a,b. The same happens for the restricted calculation R, which means that this is caused solely by the restrictions. The complete calculation C quickly increases with Θ , fig. 5a, which justifies our initial assumption that this limit needs to be very small. For the twist angle ω we observe a progressive reduction of the average radius $\langle r \rangle$ after $\omega = 0.02$. For larger angles, $\langle r \rangle$ tends towards the equilibrium radius r_0 , which is consistent with the idea that for larger angles the helix can not separate without unwinding.

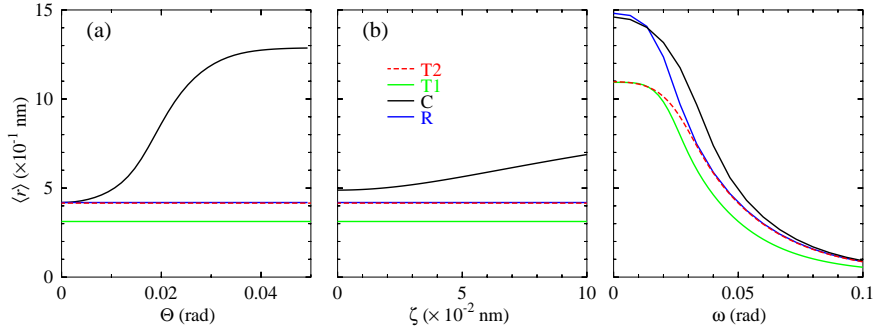


Figure 5: Average radius $\langle r \rangle$ as function of the upper limit (a) Θ , (b) ζ and (c) ω , at temperature 300 K and $\omega = 0.05$ rad; for C (black), R (blue), T1 (green) and T2 (red). Integration limits are (a,b) $b = 20$ nm, (c) $b = 15$ nm, and (a) $\zeta = 10^{-2}$ nm or (b) $\Theta = 0.01$ rad.

4. Conclusions

We have developed and tested several approximations that allow the 3D Hamiltonian to be integrated with the transfer integral (TI) method. A very sharp transition is observed, much steeper than for any harmonic or anharmonic 2D model. The new model can be used within the framework of the TI method that already exist for the 2D models [33]. The inclusion of rise distances in a setting which is more similar to the B-DNA will allow the development of new applications of the PB models, for instance to describe fluorescence resonance energy transfer (FRET) related distances in DNA [34].

5. Supplementary Information

Supplementary equations (S1–S4) are the T2 algebraic development. Supplementary figure S1 is the T2 equivalent of figure 2, and figure S2 the T2 equivalent of figure 3.

6. Acknowledgements

This work was supported by Fundação de Amparo a Pesquisa do Estado de Minas Gerais (Fapemig); Conselho Nacional de Desenvolvimento Científico e Tecnológico (CNPq); and Coordenação de Aperfeiçoamento de Pessoal de Nível Superior (CAPES).

References

References

- [1] B. Zimm, J. Bragg, Theory of the One-Dimensional Phase Transition in Polypeptide Chains, *The Journal of Chemical Physics* 28 (6) (1958) 1246–1247.
- [2] B. H. Zimm, Theory of melting of the helical form in double chains of the DNA type, *The Journal of Chemical Physics* 33 (5) (1960) 1349–1356.
- [3] J. Singh, P. K. Purohit, Structural transitions in torsionally constrained DNA and their dependence on solution electrostatics, *Acta Biomaterialia* 55 (2017) 214–225.
- [4] M. Peyrard, A. R. Bishop, Statistical Mechanics of a Nonlinear Model for DNA denaturation, *Phys. Rev. Lett.* 62 (23) (1989) 2755–2757.
- [5] G. Weber, N. Haslam, N. Whiteford, A. Prügél-Bennett, J. W. Essex, C. Neylon, Thermal Equivalence of DNA Duplexes Without Melting Temperature Calculation, *Nat. Phys.* 2 (2006) 55–59, doi:10.1038/nphys189.
- [6] G. Weber, J. W. Essex, C. Neylon, Probing the Microscopic Flexibility of DNA from Melting Temperatures, *Nat. Phys.* 5 (2009) 769–773, doi:10.1038/nphys1371.
- [7] G. Weber, Finite enthalpy model parameters from DNA melting temperatures, *Europhys. Lett.* 96 (2011) 68001, doi:10.1209/0295-5075/96/68001, URL <http://iopscience.iop.org/0295-5075/96/6/68001>.
- [8] R. V. Maximiano, G. Weber, Deoxyinosine Mismatch Parameters Calculated with a Mesoscopic Model Result in Uniform Hydrogen Bonding and Strongly Variable Stacking Interactions, *Chem. Phys. Lett.* 631–632 (2015) 87–91, doi:10.1016/j.cplett.2015.04.045.
- [9] T. D. Amarante, G. Weber, Evaluating hydrogen bonds and base stackings of single, tandem and terminal GU in RNA mismatches with a mesoscopic model, *J. Chem. Inf. Model.* 56 (1) (2016) 101–109, doi: 10.1021/acs.jcim.5b00571, URL <http://dx.doi.org/10.1021/acs.jcim.5b00571>.
- [10] E. d. O. Martins, V. B. Barbosa, G. Weber, DNA/RNA hybrid mesoscopic model shows strong stability dependence with deoxypyrimidine content and stacking interactions similar to RNA/RNA, *Chem. Phys. Lett.* 715C (2019) 14–19, doi:10.1016/j.cplett.2018.11.015.
- [11] T. Dauxois, Dynamics of breather modes in a nonlinear helicoidal model of DNA, *Phys. Lett. A* 159 (8-9) (1991) 390–395.
- [12] J. A. Cuesta, A. Sánchez, General non-existence theorem for phase transitions in one-dimensional systems with short-range interactions, and physical examples of such transitions, *J. Stat. Phys.* 115 (314) (2004) 869–893.
- [13] S. Cocco, R. Monasson, Statistical mechanics of torque induced denaturation of DNA, *Phys. Rev. Lett.* 83 (1999) 5178–81.
- [14] M. Barbi, S. Cocco, M. Peyrard, Helicoidal model for DNA opening, *Phys. Lett. A* 253 (1999) 358–369.
- [15] T. D. Amarante, G. Weber, Analysing DNA Structural Parameters using a Mesoscopic Model,

- J. Phys.: Conf. Ser. 490 (1) (2014) 012203, doi:10.1088/1742-6596/490/1/012203, URL <http://iopscience.iop.org/1742-6596/490/1/012203>.
- [16] E. W. Montroll, Statistical mechanics of nearest neighbor systems, *J. Chem. Phys.* 9 (9) (1941) 706–721.
- [17] W. K. Olson, M. Bansal, S. K. Burley, R. E. Dickerson, M. Gerstein, S. C. H. U. Heinemann, X.-J. Lu, S. Neidle, Z. S. H. Sklenar, M. Suzuki, C.-S. Tung, E. W. C. Wolberger, H. M. Berman, A Standard Reference Frame for the Description of Nucleic Acid Base-pair Geometry, *J. Mol. Biol.* 313 (2001) 229–237.
- [18] M. Barbi, S. Lepri, M. Peyrard, N. Theodorakopoulos, Thermal denaturation of a helicoidal DNA model, *Phys. Rev. E* 68 (2003) 061909.
- [19] T. Michoel, Y. Van de Peer, Helicoidal transfer matrix model for inhomogeneous DNA melting, *Physical Review E* 73 (1) (2006) 011908.
- [20] C. B. Tabi, A. Mohamadou, T. C. Kofané, Modulational instability and exact soliton solutions for a twist-opening model of DNA dynamics, *Phys. Lett. A* 373 (29) (2009) 2476–2483.
- [21] S. Behnia, M. Panahi, A. Akhshani, A. Mobaraki, Mean Lyapunov exponent approach for the helicoidal Peyrard–Bishop model, *Phys. Lett. A* 375 (41) (2011) 3574–3578.
- [22] G. Torrellas, E. Maciá, Twist–radial normal mode analysis in double-stranded DNA chains, *Phys. Lett. A* 376 (45) (2012) 3407–3410.
- [23] M. Zoli, Twisting short dsDNA with applied tension, *Physica A* 492 (2018) 903–915.
- [24] S. Zdravković, D. Chevizovich, A. N. Bugay, A. Maluckov, Stationary solitary and kink solutions in the helicoidal Peyrard-Bishop model of DNA molecule, *Chaos* 29 (5) (2019) 053118.
- [25] S. K. Nomidis, E. Skoruppa, E. Carlon, J. F. Marko, Twist-bend coupling and the statistical mechanics of the twistable wormlike-chain model of DNA: Perturbation theory and beyond, *Phys. Rev. E* 99 (3) (2019) 032414.
- [26] E. d. O. Martins, G. Weber, An asymmetric mesoscopic model for single bulges in RNA, *J. Chem. Phys.* 147 (2017) 155102, doi:10.1063/1.5006948.
- [27] Y.-L. Zhang, W.-M. Zheng, J.-X. Liu, Y. Z. Chen, Theory of DNA melting based on the Peyrard-Bishop model, *Phys. Rev. E* 56 (6) (1997) 7100–7115.
- [28] G. Weber, N. Haslam, J. W. Essex, C. Neylon, Thermal Equivalence of DNA Duplexes for Probe Design, *J. Phys.: Condens. Matter* 21 (2009) 034106, doi:10.1088/0953-8984/21/3/034106.
- [29] G. Weber, Sharp DNA denaturation due to solvent interaction, *Europhys. Lett.* 73 (5) (2006) 806–811, doi:10.1209/epl/i2005-10466-6.
- [30] T. Dauxois, M. Peyrard, A. R. Bishop, Entropy-driven DNA denaturation, *Phys. Rev. E* 47 (1) (1993) R44–R47.
- [31] K. Drukker, G. Wu, G. C. Schatz, Model simulations of DNA denaturation dynamics, *J. Chem. Phys.* 114 (1) (2001) 579–590.
- [32] K. Wendler, J. Thar, S. Zahn, B. Kirchner, Estimating the hydrogen bond energy, *J. Phys. Chem. A* 114 (35) (2010) 9529–9536.

- [33] G. Weber, TfReg: Calculating DNA and RNA Melting Temperatures and Opening Profiles with Mesoscopic Models, *Bioinformatics* 29 (2013) 1345–1347, doi:10.1093/bioinformatics/btt133, URL <http://bioinformatics.oxfordjournals.org/content/29/10/1345>.
- [34] A. Iqbal, S. Arslan, B. Okumus, T. J. Wilson, G. Giraud, D. G. Norman, T. Ha, D. M. Lilley, Orientation dependence in fluorescent energy transfer between Cy3 and Cy5 terminally attached to double-stranded nucleic acids, *Proc. Natl. Acad. Sci. USA* 105 (32) (2008) 11176–11181.